

# THE WIND MAGNETIC FIELD INVESTIGATION

R. P. LEPPING, M. H. ACÚNA, L. F. BURLAGA, W. M. FARRELL and J. A. SLAVIN  
*Laboratory for Extraterrestrial Physics, NASA/Goddard Space Flight Center, Greenbelt,  
MD 20771, U.S.A.*

K. H. SCHATTEN  
*Division of Atmospheric Sciences, National Science Foundation, Washington, DC 20550, U.S.A.*

F. MARIANI  
*Dipartimento di Fisica, Università Tor Vergata, Roma 00173, Italy*

N. F. NESS  
*University of Delaware, Bartol Research Institute, Newark, DE 19716, U.S.A.*

F. M. NEUBAUER  
*Institut für Geophysics und Meteorologie der Universität zu Köln, 500 Köln-41, Germany*

Y. C. WHANG  
*Department of Mechanical Engineering, The Catholic University of America, Washington, DC  
20064, U.S.A.*

and

J. B. BYRNES, R. S. KENNON, P. V. PANETTA, J. SCHEIFELE and E. M. WORLEY  
*Laboratory for Extraterrestrial Physics, NASA/Goddard Space Flight Center, Greenbelt,  
MD 20771, U.S.A.*

(Received 16 March, 1993)

**Abstract.** The magnetic field experiment on WIND will provide data for studies of a broad range of scales of structures and fluctuation characteristics of the interplanetary magnetic field throughout the mission, and, where appropriate, relate them to the statics and dynamics of the magnetosphere. The basic instrument of the Magnetic Field Investigation (MFI) is a boom-mounted dual triaxial fluxgate magnetometer and associated electronics. The dual configuration provides redundancy and also permits accurate removal of the dipolar portion of the spacecraft magnetic field. The instrument provides (1) near real-time data at nominally one vector per 92 s as key parameter data for broad dissemination, (2) rapid data at 10.9 vectors  $s^{-1}$  for standard analysis, and (3) occasionally, snapshot (SS) memory data and Fast Fourier Transform data (FFT), both based on 44 vectors  $s^{-1}$ . These measurements will be precise (0.025%), accurate, ultra-sensitive (0.008 nT/step quantization), and where the sensor noise level is  $< 0.006$  nT r.m.s. for 0–10 Hz. The digital processing unit utilizes a 12-bit microprocessor controlled analogue-to-digital converter. The instrument features a very wide dynamic range of measurement capability, from  $\pm 4$  nT up to  $\pm 65\,536$  nT per axis in eight discrete ranges. (The upper range permits complete testing in the Earth's field.) In the FFT mode power spectral density elements are transmitted to the ground as fast as once every 23 s (high rate), and 2.7 min of SS memory time series data, triggered automatically by pre-set command, requires typically about 5.1 hours for transmission. Standard data products are expected to be the following vector field averages: 0.0227-s (detail data from SS), 0.092 s ('detail' in standard mode), 3 s, 1 min, and 1 hour, in both GSE and GSM coordinates, as well as the FFT spectral elements. As has been our team's tradition, high instrument reliability is obtained by the use of fully redundant systems and extremely conservative designs. We plan studies of the solar wind: (1) as a collisionless plasma laboratory, at all time scales, macro, meso and micro, but concentrating on the kinetic scale, the highest time resolution of the instrument ( $=0.022$  s), (2) as a consequence of solar energy and mass output, (3) as an external source of plasma that can couple mass, momentum, and energy to the Earth's magnetosphere, and (4) as it is modified as a consequence of its imbedded field interacting

with the moon. Since the GEOTAIL Inboard Magnetometer (GIM), which is similar to the MFI instrument, was developed by members of our team, we provide a brief discussion of GIM related science objectives, along with MFI related science goals.

## 1. Introduction

The WIND Magnetic Field Investigation (MFI) will establish the large-scale structure and fluctuation characteristics of the interplanetary magnetic field (IMF) as functions of time throughout the mission, and through correlative studies will relate them to the dynamics of the magnetosphere. This experiment will provide (1) near real-time data at nominally one vector per 92 s as 'Key Parameter Data' for project support, (2) rapid data at 10.9 vectors  $s^{-1}$  for standard analysis, and (3) snapshot memory data and Fast Fourier Transform data (FFT) based on 44 vectors  $s^{-1}$  acquired on board, working synchronously with blocks of 512 samples (FFT only) each. These measurements will be precise (0.025%), accurate ( $<0.08$  nT), and ultra-sensitive (0.008 nT  $step^{-1}$ ). The basic instrument implemented is a boom-mounted dual triaxial fluxgate magnetometer system. The outboard sensor set is mounted at the end of a 12-m boom, long enough to reduce the field of the spacecraft at that location to  $\pm 0.1$  nT or less. The dual configuration provides redundancy and permits subtraction during data processing of the dipolar part of the spacecraft field contribution to the measured magnetic field. The inboard sensor assembly is mounted on the same boom, approximately  $\frac{2}{3}$  of the distance to the outboard sensor. The digital processing unit utilizes a 12-bit A/D converter to easily resolve small amplitude fluctuations of the field, and is microprocessor controlled. It also incorporates a dedicated FFT processor, developed around high performance DSP integrated circuits, which produces a 32-channel logarithmic spectrum for each axis, synthesized from a 'raw' 256-point linear spectrum. All components of the power spectral matrices corresponding to the 32 estimates are transmitted to the ground as fast as once every 23 s (high rate) providing power and phase information together with the corresponding snapshot memory time series data. As in previous instruments developed at GSFC, high reliability is obtained by the use of fully redundant systems and extremely conservative designs. The intrinsic zero drift of the sensors is expected to be below 0.1 nT over periods of up to 6 months. Electrical 'flippers' designed to simulate a 180-deg mechanical rotation of the sensors, will be used to monitor the zero level drift associated with aging of electronic components. The use of advanced statistical techniques for estimating absolute zero levels is also planned. The instruments feature a very wide dynamic range of measurements capability, from  $\pm 4$  nT up to  $\pm 65\,536$  nT per axis in eight discrete ranges; the lowest range will be activated by ground command only, and the remaining ranges either by ground command or, most commonly, automatically. The upper range permits end-to-end testing in the Earth's magnetic field without the need for special field cancellation coils or magnetic shields.

Below we will describe in more detail the characteristics of the MFI experiment, starting with a discussion of the scientific objectives of the experiment team and ending with a description of the instrument modes of operation and the related ground data processing system. Since the GEOTAIL Inboard Magnetometer (GIM), which was developed by members of our team, is similar to the MFI instrument, this document, broadly speaking, constitutes a description of its design and function also. (However, GIM has a sample rate of 4 vectors  $s^{-1}$ , and each component is quantized to 14 bit resolution.) Prof. S. Kokubun, University of Tokyo, is the principal investigator of the GEOTAIL dual magnetometer experiment (MFG) of which GIM is a part; see Kokubun *et al.* (1990) for a description of the MFG experiment. M. H. Acuña and D. H. Fairfield of NASA/GSFC are co-investigators of the MFG experiment. After the discussion of MFI science objectives, we will provide a brief discussion of GIM related studies.

## 2. Scientific Objectives of the MFI Investigation

The MFI team's primary goals, and those of many WIND investigators in general, are (1) to contribute to the further understanding of the static and dynamic properties of the solar wind (SW) and (2) to determine or clarify how the SW and its imbedded magnetic field influence the Earth's magnetosphere. We start by listing SW features of intrinsic interest to MFI investigators with large features treated first; in the adjoining double-parentheses the range in length and time units, respectively, are given. For *large-scale* features ( $\frac{1}{2} \leftrightarrow 1$  AU, longitudinally) (50  $\leftrightarrow$  100 hr) we will be observing SW streams and field sector structure primarily, but large magnetic clouds (Burlaga, 1987) occasionally fall within this range. For *meso-scale* features ( $\frac{1}{6} \leftrightarrow \frac{1}{2}$  AU), (16  $\leftrightarrow$  50 hr) we are referring to interplanetary ejecta, the bulk of magnetic cloud observations, large loops, and plasmoids. For *micro-scale* ( $10^3 \leftrightarrow 5 \times 10^6$  km), (2.5 s  $\leftrightarrow$  3.5 hr) events we refer generally to MHD waves, including Alfvén waves, D-sheets, magnetic holes and various MHD discontinuities (e.g., tangential, rotational, and contact discontinuities). For *kinetic scale* (<25 km) (<0.06 s) features, we refer to most shock wave ramps, all the way to, and including, perpendicular fast shock ramps. In coordination with IMP-8 investigators many of these features can be observed and studied with the advantage of having two point solar wind measurements; IMP-8 magnetic field measurements are obtained with an effective sample period of 0.32 s. Below we discuss some of the specific topics of interest to members of the MFI team, in terms of studies of the solar wind as a collisionless plasma laboratory, of interest in itself, as a manifestation of solar energy and mass output, and as an external source of plasma that can couple mass, momentum, and energy to the magnetosphere. Our team is interested in all three areas, but the topics listed are certainly not meant to be exhaustive of our interests.

Recently, considerable effort has been directed toward the study of geomagnetic substorms (e.g., see Baker *et al.*, 1984, for some background; Goertz and Smith, 1989; Lui, 1991; and Fairfield, 1991, who has reviewed the recent literature concerning observations and theory on geomagnetic storms and substorms and their apparent interplanetary triggers). Such events and their causes will be the prime targets of the ISTP program. We also plan to participate in such global studies of the magnetosphere, but principally from the point of view of understanding the detailed coupling of the solar wind to the magnetosphere, with emphasis on full geomagnetic storms (Tsurutani *et al.*, 1992). An attempt to classify interplanetary trigger-events will be one of our goals. In particular, the role of interplanetary shocks and magnetic clouds on magnetospheric dynamics will be central to our interests. For example, it is well known that strong or intermediate strength interplanetary shock waves (or occasionally fast, dense, solar wind in the absence of an interplanetary shock) in the vicinity of the Earth usually cause storm sudden commencements (SSC's) at Earth (Tsurutani *et al.*, 1992). An SSC is the ground manifestation of a strong magnetohydrodynamic (MHD) wave(s) transmitted to the Earth around the onset of a geomagnetic storm. As pointed out by Smith *et al.* (1986) from their statistical survey of  $\approx 50$  shocks and SSC's near solar maximum, 1978–1980, using ISEE-3 plasma and magnetic field measurements, when an SSC was seen, a causal interplanetary shock was associated with it with an 80–90% probability, and conversely an interplanetary shock had an  $\approx 80\%$  chance of causing an SSC.

SSC phenomena were first discussed as early as 1958–1959 by Dessler (1958) and by Dessler and Parker (1959). These MHD disturbances propagate in various modes from the outer boundary of the Earth's magnetosphere, the magnetopause, where they are usually (but not necessarily) initiated by an interplanetary shock. They travel to the ground along many different paths throughout the magnetosphere, including paths that encompass the magnetotail (Sugiura, 1965). What other solar wind events trigger magnetospheric MHD waves causing SSC's and what is the detailed coupling?

An early MHD description of SSC events was given by Wilson and Sugiura (1961). They showed that the external stimulus, assumed then to be a solar particle stream, caused waves to propagate Earthward primarily by longitudinal modes in low latitudes and by transverse modes at high latitudes. A general review of possible MHD wave modes in the magnetosphere's plasma environment, represented by a two-component cold plasma, is given by Sugiura (1965).

A modern view of the cause of an SSC followed by a geomagnetic storm is usually described in terms of a 'solar-terrestrial' connection, given by the following: there is the occurrence of an impulsive solar source, which has an interplanetary manifestation at and near the Earth, whose electromagnetic features (or part of them) cause geomagnetic effects, including long or moderately long-lasting consequences and sometimes a sharp onset. The causal connections among all of these

as well as the effects themselves are of major concern. Below we discuss some of these processes and effects.

Whenever impulsively ejected solar mass from an active solar region travels to 1 AU, it is likely to have serious consequences in terms of its disruption of the interplanetary medium. The related mass usually acts as an interplanetary shock driver, provided that it moves fast enough relative to the ambient solar wind, and this flowing mass may affect the magnetosphere. One form of such solar matter was simply referred to as 'ejecta' in the early literature. More recently some authors use the term 'Coronal Mass Ejecta' (CME) referring to interplanetary ejecta that are presumably related to CME's observed in the Sun's corona; see review by Kahler (1992). This view has various proponents (e.g., Gosling *et al.*, 1991 and references therein). Another such driver at 1 AU is called a 'magnetic cloud' (Burlaga *et al.*, 1981; Goldstein, 1983; Burlaga, 1991) within which  $B_z$  usually changes smoothly, so that for approximately one half its extent (i.e., on the order of 12 hr or more)  $B_z$  is usually consistently negative, depending on the 'attitude' of the cloud, where  $B_z$  is the north-south component of the interplanetary magnetic field. The relationships among the Sun's corona, CME's, magnetic clouds, and magnetospheric responses are at present controversial. In our view this represents the need to obtain a greater understanding of the connection between the interplanetary manifestation of solar ejecta-processes and the processes themselves (hopefully partly through SOHO observations), and is less related to an understanding of the the connection between the interplanetary medium and the magnetosphere. We believe that the latter connection is much better understood, even if not in detail, because of fruitful *in-situ* solar wind and magnetosphere measurements made by past and present spacecraft. Obviously more must be done in both areas. We now concentrate on characteristics of magnetic clouds which our team has studied intensively recently.

Magnetic clouds are ideal inputs for the study of solar wind-magnetosphere-ionosphere interactions, by virtue of the slowly changing magnetic field direction with a variety of orientations, a low-level of fluctuations, and the presence of only occasional discontinuities (Burlaga *et al.*, 1990). Farrugia *et al.* (1992a, b, 1993c) demonstrated that during the passage of a magnetic cloud with steady southward magnetic fields in the magnetic cloud, the occurrence of quasi periodic substorms originated just before the magnetic field turned southward. This occurrence highlights the importance of internal energy release mechanisms as opposed to highlighting substorms driven by interplanetary fluctuations. The qualitative changes in the cellular motions in the ionosphere in response to the passage of a magnetic cloud were studied by Freeman *et al.* (1993). A role of magnetic clouds in driving day-side auroral activity at sub-cusp latitudes during the onset of day-side reconnection was established by Farrugia *et al.* (1993d). It was also shown by Farrugia *et al.* (1993a), that magnetic clouds can guide solar energetic particles from the Sun to the magnetosphere. Magnetic clouds can produce very unusual conditions in the magnetosheath, as a result of the low level of fluctuations and the

high ratio of electron to proton temperature in magnetic clouds (Farrugia *et al.*, 1993b).

The amplitude of a geomagnetic storm is not related to an interplanetary shock strength (Gonzalez and Tsurutani, 1987); it is the cloud (or CME), not the interplanetary shock, that is correlated with the main phase of the storm. (We return to the question of the influence of interplanetary shocks on the magnetosphere, below.) Independent of the terminology used to describe the interplanetary features necessary to produce the storm-trigger, a storm is expected to occur, if there is a significant solar wind pressure impulse imparted to the magnetosphere via plasma that contains southward  $B_z$  (IMF) for a long enough period of time, and (usually) a preceding interplanetary shock exists which is responsible for the SSC onset.

The importance of interactions among solar wind flows in producing enhanced magnetic fields and, in turn, unusually strong geomagnetic activity was demonstrated by Burlaga *et al.* (1987). Tsurutani *et al.* (1988) have also emphasized the importance of interactions in producing enhanced  $B_z$ . Again, if  $B_z$  is southward for a long enough period of time there is an expectation of at least a geomagnetic substorm, depending on the speed of the solar wind, the details of which are controversial. In this case, however, an interplanetary shock is usually absent. The various elements of the ISTP Program are expected to help unravel the details of geomagnetic storms and their causal connections, hopefully as never before, just as we hope to understand further the mechanisms of substorms and their detailed triggers.

We should not forget the probable influence of the  $y$ -component of the interplanetary field on the magnetosphere also, especially in the cusp region where some sub-region surface must at all times possess magnetospheric fields of opposite direction allowing the possibility of magnetic merging. For those times when POLAR or Cluster are in the appropriate regions to study the signature of such a process – or whatever process is in fact detected – we hope to participate in the associative correlative study.

We also will be interested in the detailed influence of an interplanetary shock on the magnetosphere, with or without the association of a full geomagnetic storm. The literature is replete with cases where interplanetary shocks are not followed by long periods of substantial negative  $B_z$  or other obvious solar wind storm/substorm triggers and therefore not likely to be associated with a storm/substorm (Joselyn and Tsurutani, 1990; Gosling *et al.*, 1990). Lepping *et al.* (1992) determined that the MHD signal that propagates from the magnetopause to the Earth's surface as a result of an interplanetary shock impinging on the magnetopause does so with an average propagation time of  $81 \pm 18$  s, and an average speed of  $580 \text{ km s}^{-1}$ , with a suggestion that the speed is latitude dependent. They used ten separate cases of well determined interplanetary shock normals and speeds using plasma and magnetic field data from the single spacecraft, IMP-8, and the Vinas and Scudder (1986) shock-fitting technique.

An alternative approach to studying the MHD average wave propagation speed in the magnetosphere was taken by Wilken *et al.* (1982), where one event was studied in detail, the SSC of July 29, 1977, using six spacecraft. They found that the speed of a magnetospheric MHD signal, caused by an interplanetary shock, was transmitted from the front side magnetopause to the equatorial ionosphere at  $600 \text{ km s}^{-1}$ , consistent with the Lepping *et al.* results. However, Wilken *et al.* found that a signal propagation speed of  $910 \text{ km s}^{-1}$ , tangentially, held for the outer magnetosphere, at and beyond geostationary altitude. The constellation of ISTP spacecraft expected to participate in the Program, including Cluster, POLAR, and GOES and LANL, the geostationary spacecraft, should make possible the sorting of the various MHD wave signals and modes, at least over some limited regions, but including the tail region (GEOTAIL).

Below we list other specific interests of our team:

(1) In support of theory of slow-mode shocks, in the solar wind (Wang, 1988, 1991), in the magnetosheath (Lee *et al.*, 1991) and in the magnetosphere's plasma sheet boundary layer (Feldman *et al.*, 1987; Wang, in press), we hope to play a role in a multispacecraft study of such waves especially for the magnetotail, using data from WIND, IMP-8, and GEOTAIL.

(2) There will be long time periods of interplanetary magnetic field data available from WIND that will be free of disturbances by the Earth foreshock region because of the spacecraft's specific orbit. During these periods, studies of weak but steady signals for the discovery of ion pick-up generated waves due to ionization of interstellar neutrals near the orbit of Earth might be possible using advanced spectral techniques. The claim of the detection of interstellar pick-up hydrogen has been made (Gloeckler *et al.* 1993) and apparently associated waves in the magnetic field also observed (Smith, 1993) – both from measurements on board the *Ulysses* spacecraft at 5 AU; see Lee and Ip (1987).

(3) Also there will be limited time intervals available when WIND is downstream of the moon where pickup ions of lunar origin have been observed streaming perpendicular to the interplanetary magnetic field (Hilchenbach *et al.*, 1992). Since these particles can produce weak fluctuation fields via pick-up driven plasma instabilities, some interesting studies may be possible, somewhat analogous to those of solar wind-comet interactions; for examples, see the March 1986 special issue of *Geophysical Research Letters on Comets*.

(4) The WIND spacecraft also has the potential of contributing to truly 3D solar wind studies in combination with the *Ulysses* spacecraft, which will move between the southern and northern polar regions of the Sun during the primary phase of the WIND mission.

(5) With the WIND spacecraft still active after the launch of the CLUSTER array of spacecraft and when CLUSTER is located in the solar wind, interesting studies of spatial and temporal variations of the interplanetary medium will be possible. The CLUSTER array and the WIND spacecraft will form a 'two-station' array with spatial resolution available in the direction of the connecting vector. Studies with

the CLUSTER array in and outside the foreshock region will be considered. IMP-8 measurements may augment this scheme contributing data from a 'three-station array'.

(6) Finally, although WIND will be in the Earth's magnetosheath and magnetosphere for a small percentage of time in this mission, we will nevertheless utilize the associated data, as much as possible, to analyze these regions. For example, there will be an opportunity to study further the bow shock, magnetopause, and associated boundary layer plasmas, again in coordination with other ISTP spacecraft teams.

### 3. GIM Related Observations and Studies

GEOTAIL observations will be carried out in two main phases (and possibly a third phase, or a repeat of the first phase); (1) the deep tail will be observed for about 2.3 years with so-called double-lunar swing-by orbits (approximately figure 8's) to an apogee of about  $220 R_e$ ; (2) then the apogee drops to about  $60 R_e$  (yet to be determined) into an elliptical orbit for studies closer to Earth, optimizing near-tail region studies. One of the main goals of the GSFC magnetic field team is to obtain a greater understanding of tail structure through a general survey of the tail to relatively large distances (about  $220 R_e$ ) with the possibility of having, at least part of the time, two point measurements when IMP-8 (apogee about  $37 R_e$ ) is in the near tail region, or have at least single point measurements (when it is tracked). Especially important will be observations of tail dynamic changes during active periods. As discussed by Kokubun *et al.* (1990) the changes can again be ordered by the scale size of the current system causing the change, i.e., ordered from macroscopic currents to plasma waves and discontinuities (MP) to shocks; the bow shock, for example, will be studied by GEOTAIL. Macroscopic currents include MP currents, ring current, tail neutral-sheet currents, and field-aligned currents that couple the magnetospheric plasma to the ionosphere. As Kokubun *et al.* point out, the monitoring of the magnetic field configuration changes associated with these current systems is imperative for the understanding of the global magnetospheric transport of mass, momentum, and energy during storms and substorms.

Recently, much attention has been given to the formation and transport of a magnetotail temporal structure, called a plasmoid, which is believed to have an approximately oval cross-section in the  $(X - Z)_{\text{GSM}}$  plane, and is intimately associated with the substorm. This plasmoid picture is not fully accepted, however. Among those who generally accept the existence of a tail plasmoid, some believe that is the result of magnetic field-line merging at various points in the magnetosphere, including those at the front and rear of the plasmoid itself. Estimates of plasmoid sizes vary, but on average they have been determined to have a length of about  $60 R_e$  in the near/middle tail region (Richardson *et al.*, 1987). But in the near tail region there is some evidence that plasmoids as small as  $8 R_e$  may exist

(Slavin *et al.* 1990; Moldwin and Hughes, 1991, 1992). Presently it is believed that the plasmoid changes in various ways but does not change much in size, as it propagates down the tail. Examining these objects and tracking their evolution with time or distance down the tail will be one of the goals of the studies of Earth's dynamic tail by the magnetic field team. Studying the properties of the tail on finer time scales will also be important. These include plasma wave studies in the ELF range. Other studies also include those associated with the tail boundary, for example, flux-transfer events, MP surface waves, and near-MP plasma features related to boundary layer plasma – all of these are important also for near tail studies, and perhaps are even more relevant there. As Kokubun *et al.* also point out, in the near tail orbit, the spacecraft will skim along the MP for long periods enabling these kinds of MP-related studies, including those generally associated with multiple boundary crossings. Hopefully, in the near-tail orbit the spacecraft will spend a long period of time (near its apogee) in an active near-tail region which would maximize information on the tail's early response to the substorm trigger and on front-side plasmoid formation.

#### 4. MFI Instrumentation Description

The basic instrumentation selected for the WIND Magnetic Field Investigation (MFI) is based on the magnetometers previously developed for the Voyager, ISPM, GIOTTO, and Mars Observer missions which represent state-of-the-art instruments with unparalleled performance. Table I summarizes the principal instrument characteristics. The basic configuration consists of dual, wide range ( $\pm 0.001$  to  $\pm 65\,536$  nT) triaxial fluxgate magnetometers mounted remote from the spacecraft body on a deployable boom, a 12-bit resolution A/D converter system and a microprocessor controlled data processing and control unit (DPU). The outer magnetometer sensor is mounted at the end of the boom while the inner unit is located approximately midway between the outer one and the main body of the spacecraft. This configuration allows the real-time estimation and elimination of the dipolar components of the spacecraft-generated magnetic field in order to obtain a more accurate ambient field.

A block diagram of the MFI instrumentation is shown in Figure 1. The advantages of the dual magnetometer approach for weak magnetic field measurements like those associated with the IMF, have been proven over many space missions since their original introduction by Ness *et al.* (1971). The 12 m long deployable boom is of the 'astromast' type and places the sensors at two different radial distances from the center of the spacecraft while the signal processing electronics package is mounted on the main spacecraft body.

The dual magnetometer system is supported by the fully redundant DPU which interfaces with the spacecraft data and power systems. The use of full redundancy in the MFI instrument is an important feature that emphasizes the critical nature of the

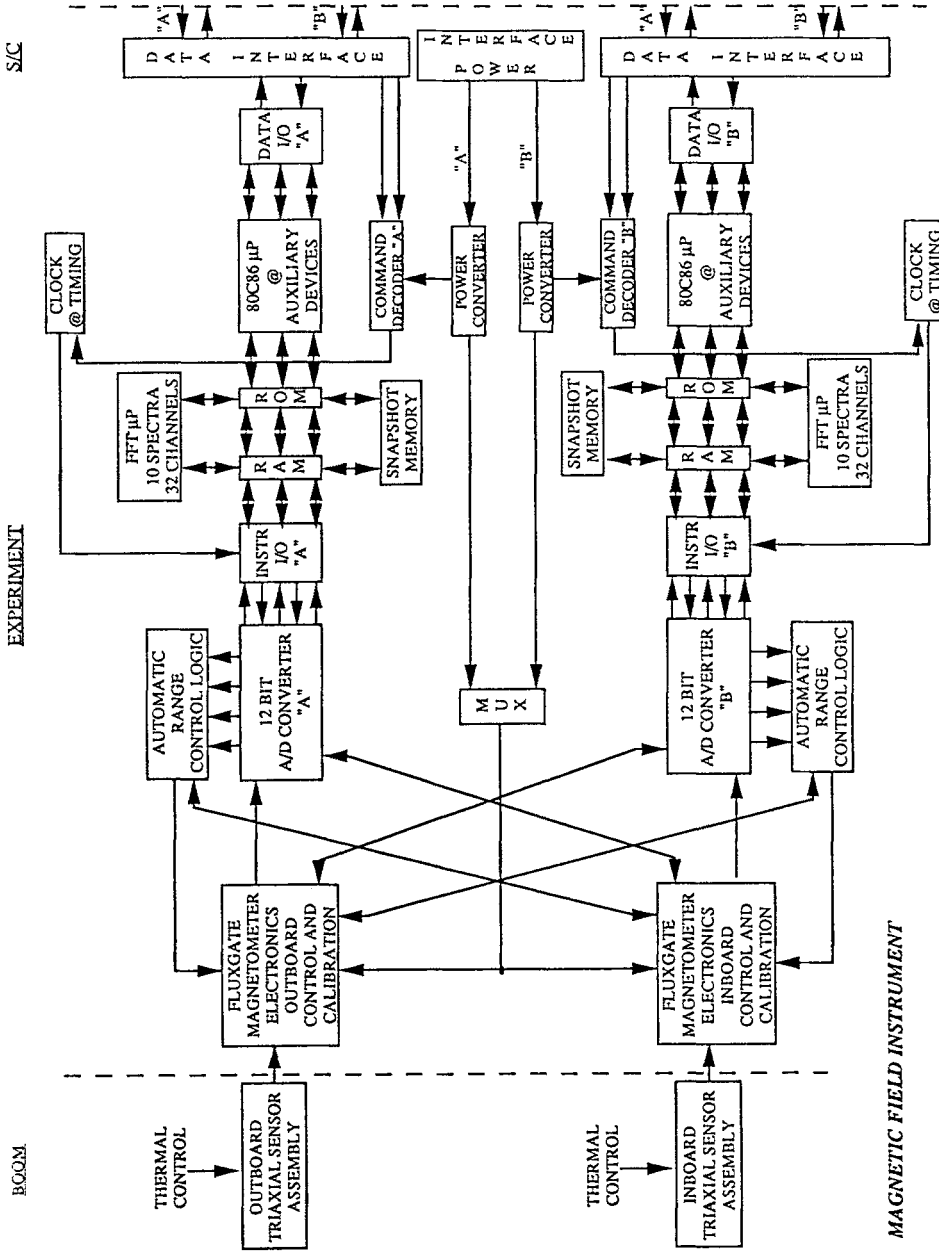


Fig. 1. Block diagram of the MFI magnetic field experiment.

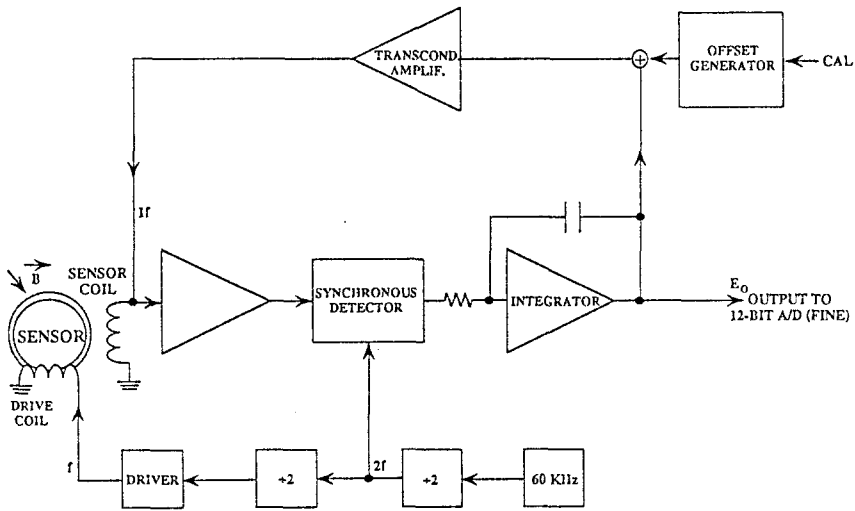
MAGNETIC FIELD INSTRUMENT

TABLE I  
Summary of instrument characteristics

Instrument type	Dual, triaxial fluxgate magnetometers (boom mounted)
Dynamic ranges (8)	$\pm 4$ nT by ground command; $\pm 16$ nT; $\pm 64$ nT; $\pm 256$ nT; $\pm 1024$ nT; $\pm 4096$ nT; $\pm 16,384$ nT; $\pm 65,536$ nT
Digital resolution (12-bit A/D)	$\pm 0.001$ nT; $\pm 0.004$ nT; $\pm 0.016$ nT; $\pm 0.0625$ nT; $\pm 0.25$ nT; $\pm 1.0$ nT; $\pm 4.0$ nT; $\pm 16.0$ nT
Sensor noise level	$< 0.006$ nT r.m.s., 0–10 Hz
Sampling rate	44 vector samples $s^{-1}$ in snapshot memory and 10.87 vector samples $s^{-1}$ standard
Signal processing	FFT processor, 32 logarithmically spaced channels, 0 to 22 Hz. Full spectral matrices generated every 46 s (low rate) or 23 s (high rate) for four time series ( $B_x$ , $B_y$ , $B_z$ , $ B $ ).
FFT windows/filters	Full de-spin of spin plane components, 10% cosine taper, Hanning window, first difference filter
FFT dynamic range	72 dB, $\mu$ -law log-compressed, 13-bit normalized to 7-bit + sign
Sensitivity threshold	$\simeq 0.5 \times 10^{-3}$ nT/ $\sqrt{\text{Hz}}$ in range 0.
Snapshot memory capacity	256 Kbits
Trigger modes (3)	Overall magnitude ratio, directional max–min peak to peak change, spectral increase across frequency band (r.m.s.)
Telemetry modes	Three, selectable by ground command
Mass	Sensors (2): 450 g Electronics (redundant): 2100 g
Power consumption	2.4 W

magnetic field measurements for the achievement of the WIND and ISTP science objectives. It significantly reduces the probability of failures and takes advantage of the inherent redundancy provided by the dual magnetometer configuration. This redundancy includes assigning by ground command either primary or secondary data stream for the outer sensor and likewise for the inner sensor. In addition to the block redundancy provided, each magnetometer system incorporates self-resetting electronic ‘fuses’ which isolate the common subsystems in case of catastrophic problems.

Each sensor assembly consists of an orthogonal triaxial arrangement of ring-core fluxgate sensors plus additional elements required for thermal control. The fluxgate sensors are the latest in a series developed for weak magnetic field measurements by Acuña (1974) and which have been extensively used in missions like VOYAGER, AMPTE, GIOTTO, Mars Observer, CLUSTER, etc. due to their superior performance and low power consumption. The detailed principles of operation of fluxgate magnetometers are well known and will not be repeated here. It is sufficient to refer to Figure 2 for a simplified description of their operation. (For additional information the reader is referred to Ness (1970) and Acuña, 1974;

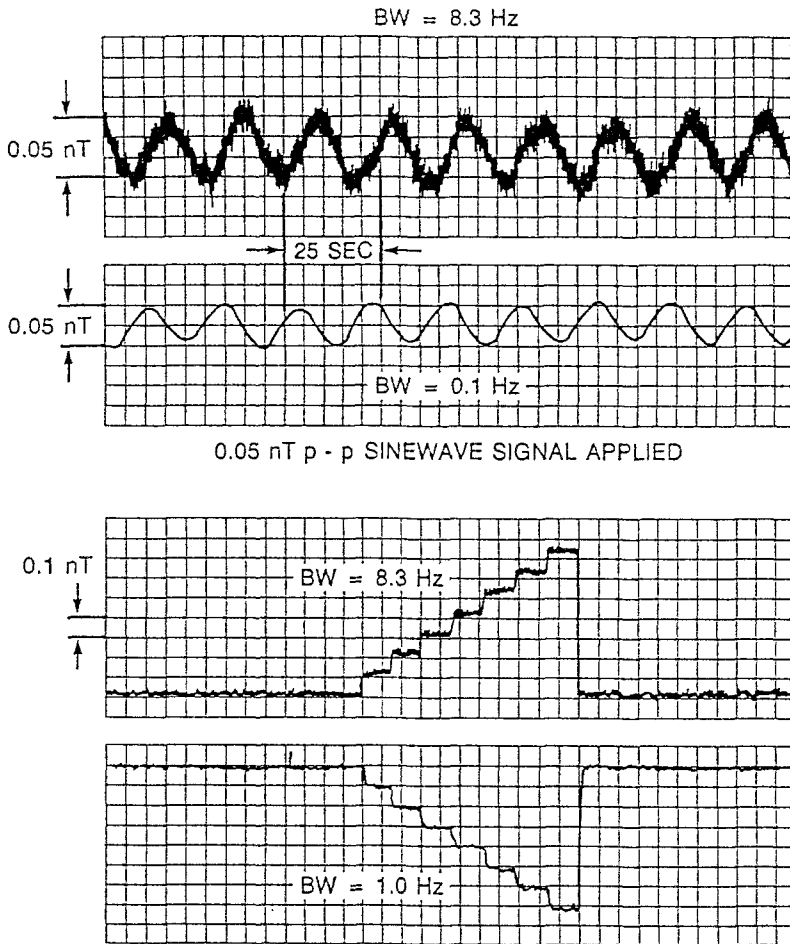


BLOCK DIAGRAM OF BASIC  
FLUXGATE MAGNETOMETER

Fig. 2. Schematic of standard fluxgate operation.

Acuña and Ness, 1976a, b.) As shown in the figure the fluxgate sensors are driven cyclically to saturation by a 15 KHz signal derived from the DPU master clock. The sensor drive signals are derived from an efficient high energy storage system which is capable of driving the ring core sensors to peak excitations which are more than 100 times the coercive saturation force of the cores. This type of excitation eliminates from consideration many 'perming' problems which have been attributed to fluxgate sensors in the past. In the absence of an external magnetic field, the fluxgate sensors are 'balanced' and no signal appears at the output terminals. When an external field is applied, the sensor balance is disturbed and a signal containing only even harmonics of the drive frequency appears at the output of the sensors. After amplification and filtering, this signal is applied to a synchronous detector and high gain integrating amplifier which is used to generate a current proportional to the magnitude of the applied field which is fed-back to the sensor to *null* the effective magnetic field seen by it. The output of a single axis magnetometer is then a voltage proportional to the magnitude, direction and polarity of the ambient magnetic field with respect to the sensor axis orientation. A triaxial magnetometer is thus created when three single axis sensors are arranged in an orthogonal configuration and three sets of signal processing electronics are used to produce three output voltages proportional to the orthogonal components of the ambient magnetic field.

The noise performance of the MFI fluxgate sensors is shown in Figures 3(a) and 3(b). Total r.m.s. noise level over the 0-10 Hz band does not exceed 0.006 nT. This noise level is several orders of magnitude below the lowest recorded levels of



## WIND PROTOTYPE SENSOR

Fig. 3a. MFI fluxgate noise performance graphs.

IMF fluctuations at 1 AU and is more than adequate to properly detect and identify all magnetic field phenomena of interest to MFI.

The six analog signals generated by the Outboard (OB) and Inboard (IB) magnetometers are digitized by the 12-bit successive approximation A/D converter. The 12-bit resolution allows the recovery of a very large dynamic range of signals spanning 72 dB. To further increase the measurement dynamic range and to accommodate simplified integration and test requirements during spacecraft testing, the dynamic range of the magnetometers can be changed automatically if the magnitude of the measured signals exceeds or drops below established digital

## WIND PROTOTYPE SENSOR

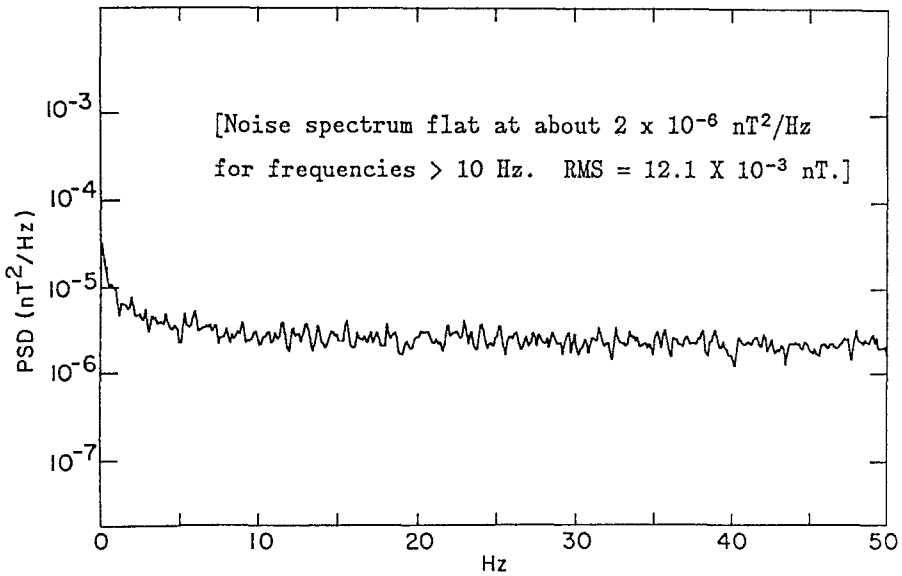
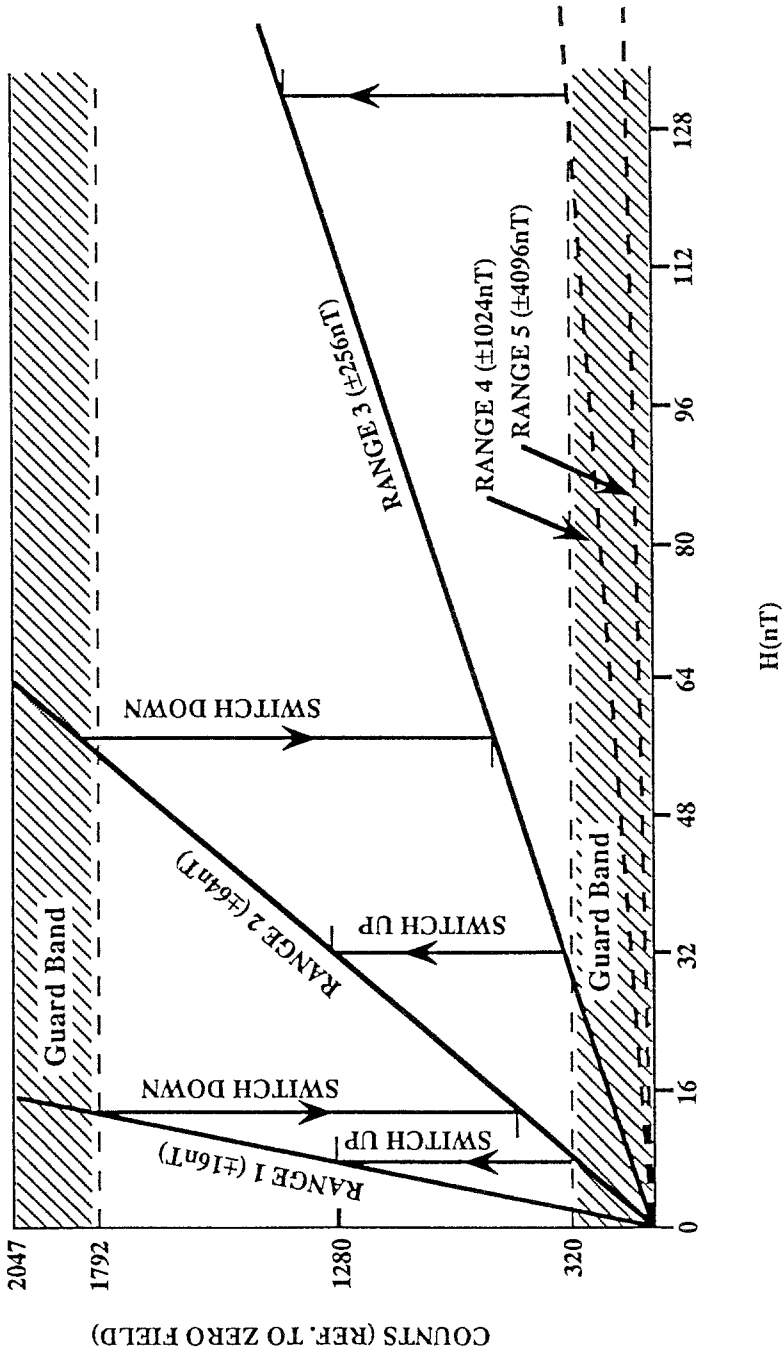


Fig. 3b. Noise power spectrum for MFI prototype sensor.

thresholds illustrated in Figure 4. In this fashion, the MFI instrumentation can cover eight orders of magnitude in magnetic field measurement capability, from 0.001 to 65 536 nT per axis. The operation of the automatic ranging system is controlled by the microprocessor and allowed only at clearly defined times in the telemetry frame to avoid ambiguities in the interpretation of the data. When the digitized output of any magnetometer axis exceeds  $\frac{7}{8}$ 's of full scale, the microprocessor generates a command to step up (increase) the magnetometer to the next, less sensitive, range. Conversely, when the output of all axes drops below  $\frac{1}{8}$ th of full scale, the DPU commands the appropriate magnetometer to step down (decrease) to the next most sensitive range. A 'guard band' of  $\frac{1}{8}$ th scale is provided to avoid the loss of measurements due to saturation until the range is updated. The decision to increase or decrease dynamic range is made at the basic internal sampling rate of 44 vectors  $\text{s}^{-1}$ . (At this same rate, the Outboard sensor magnetic field data is distributed to the rest of the WIND instruments.) However, the MFI telemetry allocation is not sufficient to allow the transmission of all the data to the ground, so on-board data averaging, compression, and decimation must be used to reduce the 'raw' rate to an acceptable value. These operations are described in more detail later on in this paper. The DPU also controls calibration sequences which provide the necessary currents to determine the scale factor of each of the Outboard and Inboard magnetometer axes for various dynamic ranges as well as the determination of zero offsets associated with the electronics by implementing a  $180^\circ$  phase reversal of the signals processed (electronic 'flipping').



*Range Switching - Magnetic Field Experiment*

Fig. 4. Range switching scheme.

## 5. Digital Processing Unit

The DPU, including the analog-to-digital converter, is based on the concept of a 'smart system' which performs all required operations: data manipulation and formatting, averaging, compaction and decimation, etc. The basic microprocessor used is a radiation hardened version of the popular 80C86, provided by the ISTP Project Office to the experimenters, and a block diagram of the DPU architecture is shown in Figure 1. All core operations performed by the system are carried out under the control of interrupt driven software synchronized to the telemetry system clock, subframe and frame rates. The system design is based on a default executive and processing program which is stored and executes in Read-Only-Memory (ROM). All subsequent operations are carried out from ROM and no commands or memory loads are required to obtain valid data from the instrument after initial turn-on. All default parameter values for the system are stored in tables in ROM which, once mapped into RAM during initialization, can later be modified by ground commands to update calibrations, alignments, sampling rates, zero levels, etc.

The execution of the executive and auxiliary programs is monitored by hardware and software watchdog timers. The external hardware watchdog timer is normally reset by proper execution of the executive program; in the absence of a reset pulse, the watchdog timer will reset the DPU and restart the default ROM program, reloading all default parameters from ROM.

In addition to the core DPU functions described above, to better enable the study of rapid changes in the ambient magnetic field, the MFI instrumentation includes two additional functional elements designed specifically for this purpose: (a) a 256 kbit 'Snapshot Memory' and (b) a Fast Fourier Transform Processor (FFT) implemented around a TI320C10 dedicated digital signal processor and associated memory. This enables the study of the physics of the fine-scale structure of shock waves, directional discontinuities and boundary structures, as well as the various wave modes and non-coherent fluctuations occurring in the solar wind. The snapshot memory can be programmed to trigger upon the occurrence of one or more of the three classes of conditions:

(1) A magnetic field magnitude jump, especially important for some kinds of shock ramp measurements.

(2) A directional change (peak to peak), useful for measurements of transition regions of directional discontinuities (tangential and rotational).

(3) Changes in the characteristics of field fluctuations over time, useful for some kinds of wave studies on the kinetic scale.

When the selected condition is satisfied, the contents of the snapshot memory are 'frozen'. Under normal conditions, Outboard magnetometer data sampled at the highest possible rate ( $44 \text{ samples s}^{-1}$ ) is circulated through the snapshot memory with cyclical overwriting once the memory is full. Thus a maximum of 7282 vectors can be stored in memory. This corresponds to approximately 165 s of data or 2 min

45 s. The use of memory pointers in the DPU software allows the recovery of data acquired 82 s *prior* to the occurrence of the trigger (i.e., one-half of the buffer). Thus it is possible to study precursor events in high time resolution.

The FFT processor complements the snapshot memory by providing full spectral estimation capabilities in the frequency range of 0–22 Hz for Primary magnetometer data. The basic FFT engine produces raw spectral estimates of the three components of the field in 256 spectral bands using 512 samples of the ambient magnetic field data (i.e. 11.6 s). In addition, the processor computes the magnitude of the magnetic field vectors in the time series being analyzed, its Fast Fourier Transform and the cross-spectral estimates associated with the three orthogonal components. In order to reduce the effects of the large signals associated with the spacecraft spin, the TI320C10 processor is used to de-spin the spin plane components of the data prior to the computation of the FFT for these axes. Other functions included in the FFT processor are pre-whitening of input data, windowing (cosine taper and Hanning), and data compression. The latter is required to reduce the volume of raw data produced by the spectral analysis (256, 3X3 spectral matrices plus a 256 element time series) to a manageable size which can be accommodated by the allocated telemetry rate to MFI. In the frequency domain, the 256 spectral estimates are compressed into 32 logarithmically spaced frequency bands of constant fractional bandwidth (or equal 'Q' filters). In the amplitude domain, the 12-bit data are logarithmically compressed to 7-bits plus sign using two alternate schemes: (a) a variable MSB truncation approach and (b) an algorithm based on the  $\mu$ -Law commonly used in communication systems. The net result is a set of 32 full spectral matrices for the components and 32 spectral estimates for the field magnitude, transmitted to ground using 8-bit words but representing the original dynamic range of 12-bits. Further details of the FFT processor can be found in Panetta *et al.* (1991, 1992a, b).

Finally, the DPU supports the distribution of high time resolution data to other experiments aboard the spacecraft through the Command and Attitude Processor (CAP). A serial data stream consisting of zero corrected primary magnetometer data sampled at 44 samples per second, plus ancillary range and miscellaneous information, is provided to the spacecraft CAP which in turn distributes it to other instruments in one of two available formats:

(a) The original, unaltered serial stream, buffered by the CAP (highest time resolution), or

(b) Two pulse signals occurring once per spacecraft revolution (3 s), one related to the azimuth of the magnetic field in the spin plane, and the other to the elevation of the same in local spacecraft coordinates.

The nominal telemetry modes for WIND-MFI are illustrated in Table II. Three modes are used: (0) normal (default), (1) high percentage primary mag FFT, low SS, (2) similar to mode 1 with SS replacing FFT, so that FFT rate is zero. Note that the different modes allocate different fractions of the available telemetry resources to the sampling of the Outboard and Inboard magnetometers, the snapshot memory

TABLE II  
MFI telemetry modes

Data stream	Mode (0) normal (BPS)	Mode (1) 'FFT' (BPS)	Mode (2) 'SSM' (BPS)
Outboard	195.8 (5.43) <sup>a</sup>	391.3 (10.87)	391.3 (10.87)
Inboard	195.8 (5.43)	19.6 (0.54)	19.6 (0.54)
FFT	55.6	55.6	0
SSM <sup>b</sup>	31.0	13.9	69.5
H.K. status <sup>c</sup>	2.2	0.0	0.0
Total	480.4	480.4	480.4
Inst. status <sup>d</sup>	4.3	4.3	4.3
Combined	484.7	484.7	484.7

<sup>a</sup> ( ) means: vector samples  $s^{-1}$ .

<sup>b</sup> Snap-shot memory of 256 000-bit size for capture of transient events. (Basic samp rate: 44 vectors  $s^{-1}$ .)

<sup>c</sup> Housekeeping status: this includes a command counter, mode command id, major frame counter, etc.

<sup>d</sup> Instrument status: this includes telemetry mode, range status, auto/manual state, electronic flipper state, snapshot trigger id, error bits, etc.

buffer and the FFT processor. When the WIND spacecraft is located inside the Moon's orbit, the telemetry rate allocated to the experiments is doubled and the rates shown in Table II must be doubled. Mode (0) is a normal default mode which provides equal sampling rates to the outboard and inboard magnetometers. This mode will be used initially to characterize and evaluate the nature of the spacecraft generated magnetic field.

## 6. Power Converters and Thermal Control

The MFI instrumentation derives power from the 28 V regulated spacecraft bus through two redundant power converters. Only one subsystem is powered at any particular time. The converters are high efficiency units which operate at 50 KHz and are synchronized to the master crystal clock of the DPU to minimize interference to other experiments aboard the spacecraft. Selection of the active converter is simply accomplished by powering the desired unit.

To maintain the fluxgate sensors within their optimum operating temperature range, it is necessary to provide heater power to the boom mounted triaxial sensor assemblies during periods of Sun occultation. Since it is extremely difficult to reduce the stray magnetic field associated with the operation of D.C. powered foil heaters to acceptable levels for MFI, a magnetic amplifier operating at 50 KHz is used to obtain automatic, proportional control of AC power supplied to

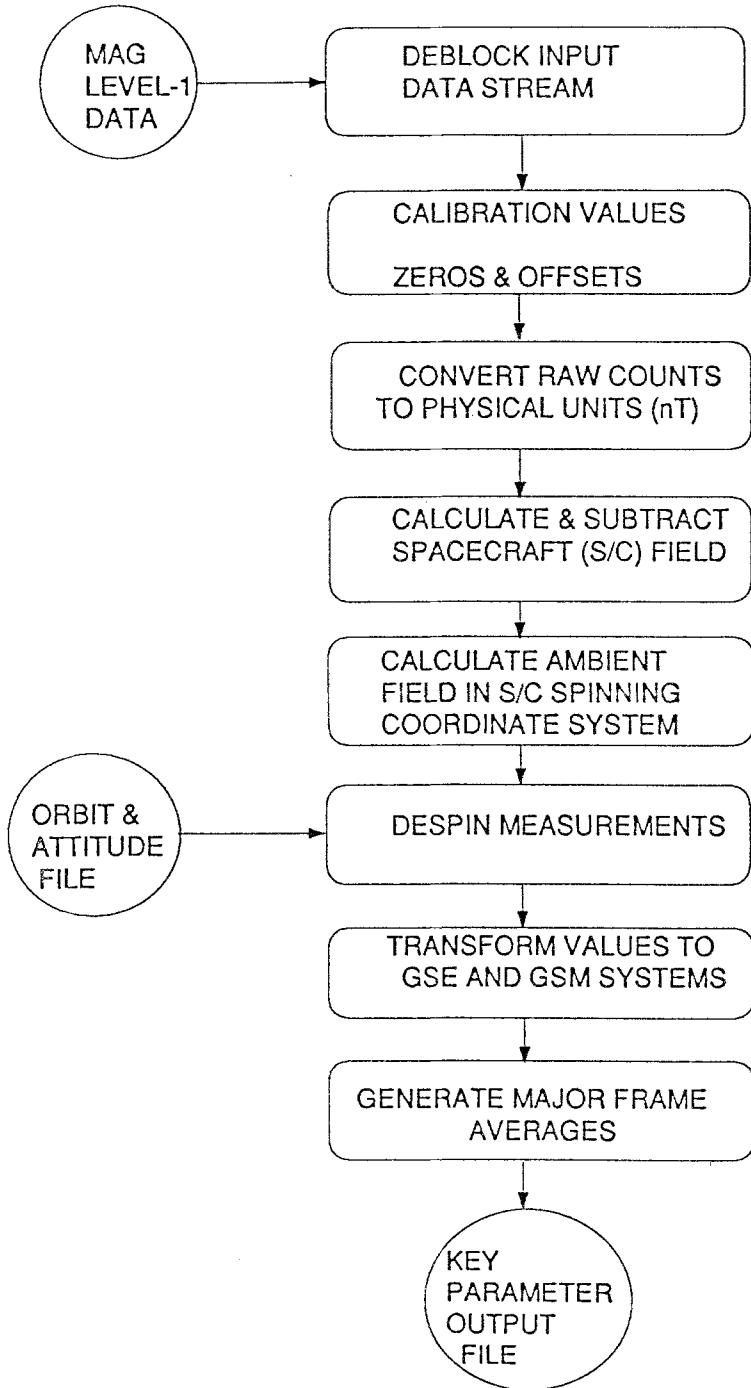


Fig. 5. MFI key parameter (K.P.) data processing system.

MFI RDAF PROCESSING SYSTEM

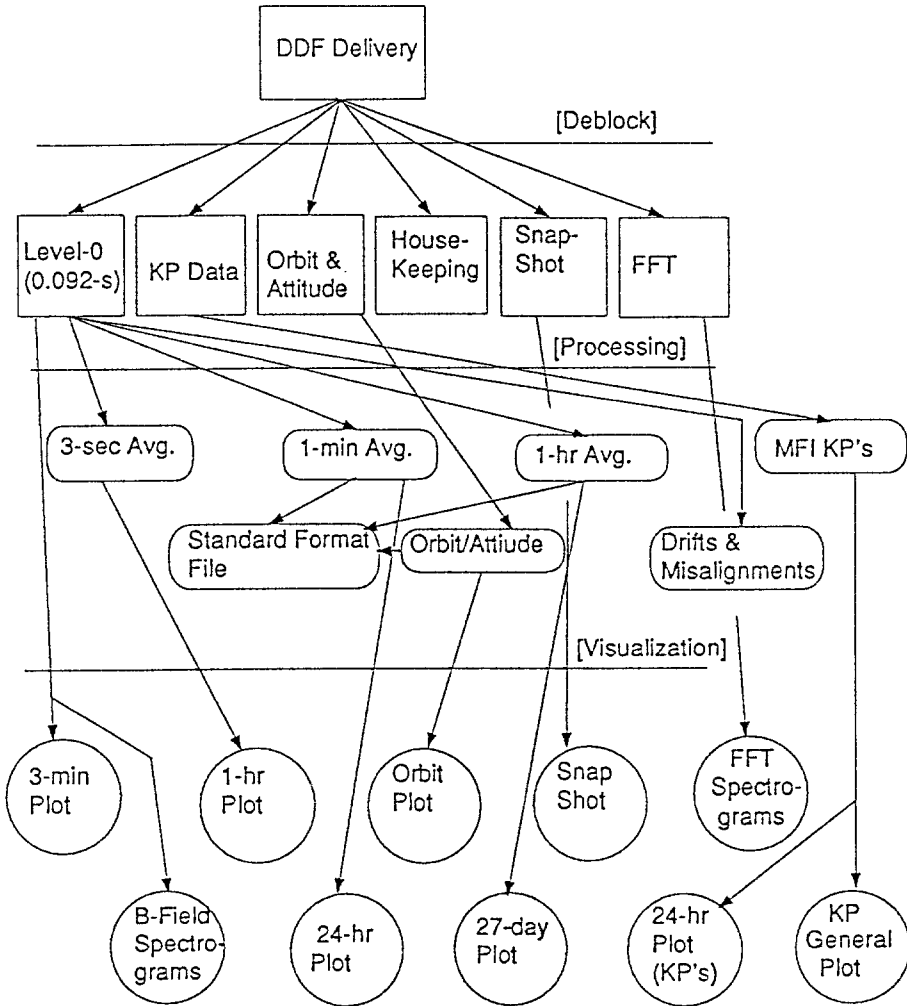


Fig. 6. MFI ground data processing system facilitated by the remote data analysis facility (RADF).

the heating elements. The nominal power required to maintain the sensors at the desired temperatures is estimated to lie in the range of 0.3 to 0.5 W.

## 7. MFI Ground Data Processing

A major consideration in the design of the experiment software and operating modes is the general requirement by the ISTP Project for investigations to produce 'Key Parameters' at low time resolution in a Central Data Handling Facility (CDHF) without the continuous intervention in the process by MFI investigators. See Figure 5 for a description of this system. In fulfilling this responsibility the MFI experiment will provide averages of the ambient magnetic field and other ancillary quantities every 92 s, the WIND spacecraft telemetry major frame duration. The in-house production data processing will be carried out on a SUN 4/380 workstation (RDAF) and the standard data products will be stored on optical discs. It is expected that CD-ROMS will be produced in common data formats for distribution to the ISTP science community. The production processing system is schematically described in Figure 6. It will produce vector field data at the rates: 44 vectors  $s^{-1}$  for snapshot and 10.87  $s^{-1}$  standardly (0.092 s) and averages at 3 s, 1 min, and 1 hr – in GSE and GSM coordinates. The data processing philosophy is similar to that used for the IMP series of magnetometer data processing (see Mish and Lepping, 1976) but with greater efficiency (Farrell *et al.*, 1994) and advanced data visualization facility.

We now briefly describe the phases of the processing program illustrated in Figure 6. Initially, deliveries are received from the Data Distribution Facility (DDF) on CD-ROM and are immediately deblocked into various files of interest. This deblocking takes place on the SUN computer with a program specifically designed to strip the requested files from the delivery CD-ROM and place them on computer harddisk. At this stage, the files contain MFI measurements in their raw, uncalibrated form. Further processing is performed to create a set of data files containing refined, averaged measurements. Processing is also performed to create a 'Standard Format File' containing magnetic field and orbit/attitude data in a simple format for shipment to NSSDC. This file can be used by other interested ISTP investigators. Finally, visualization software written in Interactive Data Language (IDL) can access these files of refined data for the creation of hourly and daily plots. Software is also written to analyze our Key Parameter deliveries. Electronic drift and sensor misalignment values of the spin plane sensors will also be stored in a data file. Drifts and misalignments of the z-sensor require a larger-scale statistical study, which will be performed jointly by our Goddard Team and Prof. Franco Mariani at the University Tor Vergata in Italy, to ensure the highest accuracy of the final product, the ambient magnetic fields, at all time-scales.

### Acknowledgement

We are grateful to Suzan Stacy for all of her generous help.

## References

- Acuña, M. H.: 1974, *IEEE Trans. Magnetics* **MAG-10**, 519.
- Acuña, M. H. and Ness, N. F.: 1976a, in T. Gehrels (ed.), *Jupiter*, University of Arizona Press, Tucson, p. 830.
- Acuña, M. H. and Ness, N. F.: 1976b, *J. Geophys. Res.* **81**, 2917.
- Baker, D. N., Akasofu, S. I., Baumjohann, W., Bieber, J. W., Fairfield, D. H., Hones, E. W., Jr., Mauk, B. H., McPherron, R. L., and Moore, T. E.: 1984, *Solar Terrestrial Physics – Present and Future*, 8-1 to 8-55.
- Burlaga, L. F.: 1991, in L. Lanzerotti, R. Schwenn, and E. Marsch (eds.), *Physics of the Inner Heliosphere*, Ch. 6, Springer-Verlag, New York.
- Burlaga, L. F., Sittler, E. C., Jr., Mariani, F., and Schwenn, R.: 1981, *J. Geophys. Res.* **86**, 6673.
- Burlaga, L. F., Behannon, K. W., and Klein, L. W.: 1987, *J. Geophys. Res.* **92**, 5725.
- Burlaga, L. F., Lepping, R. P., and Jones, J.: 1990, in C. T. Russell, E. R. Priest, and L. C. Lee (eds.), *Geophys. Monogr. Ser., Physics of Flux Ropes*, AGU, Washington, D.C., Vol. 58, p. 373.
- Dessler, A. J.: 1958, *J. Geophys. Res.* **63**, 405.
- Fairfield, D. H.: 1991, 'Advances in Magnetospheric Storm and Substorm Research: 1989–1991', Review presented at the IAGA Meeting Vienna, Austria.
- Farrell, W. M., Thompson, R. F., Lepping, R. P., and Byrnes, J. B.: 1994, *IEEE Magnetics*, in press.
- Farrugia, C. J., Freeman, M. P., and Burlaga, L. F.: 1992, *Proceedings of the International Conference on Substorms (ICS-1)*, Kiruna, Sweden ESA SP-335, p. 371.
- Farrugia, C. J., Richardson, I. G., Burlaga, L. F., Osherovich, V. A., and Lepping, R. P.: 1993a, *J. Geophys. Res.* **98**, 15497.
- Farrugia, C. J., Fitzenreiter, R. J., Burlaga, L. F., Erkaev, N. V., Osherovich, V. A., Biemat, H. K., and Fazakerly, A.: 1993b, *Adv. Space Res.* **14**(7), 105.
- Farrugia, C. J., Freeman, M. P., and Burlaga, L. F., Takahashi, K.: 1993c, *J. Geophys. Res.* **98**, 7657.
- Farrugia, C. J., Sandholt, P. E., and Burlaga, L. F.: 1993d, *J. Geophys. Res.*, submitted.
- Feldman, W. C., Tokar, R. L., Birn, J., Hones, E. W., Jr., Bame, S. J., and Russell, C. T.: 1987, *J. Geophys. Res.* **92**, 83.
- Freeman, M. P., Farrugia, C. J., Burlaga, L. F., Lepping, R. P., and Greenspan, M.: 1993, *J. Geophys. Res.* **98**, 7633.
- Gloeckler, G., Geiss, J., Fisk, L., Glavin, A., and Ipavich, F.: 1993, *Detection of Interstellar Pick-up Hydrogen in the Solar System*, submitted.
- Goertz, C. K. and Smith, R. A.: 1989, *J. Geophys. Res.* **94**, 6581.
- Goldstein, H.: 1983, *Solar Wind Five*, NASA Conference Publ. 2280, 731.
- Gonzalez, W. D. and Tsurutani, B. T.: 1987, *Planetary Space Sci.* **35**, 1101.
- Gosling, J. T., McComas, D. J., Phillips, J. L., and Bame, S. J.: 1991, *J. Geophys. Res.* **96**, 7831.
- Hilchenbach, M. et al.: 1992, *COSPAR, Program Book*, p. 260.
- Joselyn, J. A. and Tsurutani, B. T.: 1990, *EOS*, Transactions of Am. Geophys. Union, p. 1809.
- Kahler, S. W.: 1992, *Ann. Rev. Astron. Astrophys.* **30**, 113.
- Kokubun, S. et al.: 1990, *GEOTAIL Interim Report*, Institute of Space and Astronautical Science, p. 55.
- Lee, L. C., Yan, M., and Hawkins, J. G.: 1991, *Geophys. Res. Letters* **18**, 381.
- Lee, M. A. and Ip, W. H.: 1987, *J. Geophys. Res.* **92**, 11, 041.
- Lepping, R. P., Vinas, A. F., Lazarus, A. J., Sugiura, M., Araki, T., Kokubun, S., Stahara, S. S., and Spreiter, J. R.: 1992, *EOS*, Transactions of Am. Geophys. Union, p. 251.
- Lui, A. T. Y.: 1991, *J. Geophys. Res.* **96**, 1849.
- Mish, W. H. and Lepping, R. P.: 1976, NASA/GSFC X-694–76–158.
- Moldwin, M. B. and Hughes, W. J.: 1991, *EOS*, Transactions AGU, p. 242 (SME32E-3).
- Moldwin, M. B. and Hughes, W. J.: 1992, *Geophys. Res. Letters* **19**, No. 11, 1081.
- Ness, N. F.: 1970, *Space Sci. Rev.* **11**, 111.
- Ness, N. F., Behannon, K. W., Lepping, R. P., and Schatten, K. H.: 1971, *J. Geophys. Res.* **76**, 3564.
- Panetta, P. V. and Acuña, M. H.: 1991, *WIND MFI FFTP Processor Requirements Document*, Rev. 10.
- Panetta, P. V.: 1992a, *WIND MFI Telemetry Bits Definition Document*, Rev. 1.

- Panetta, P. V.: 1992b, *WIND MFI Flight Software Description Document*, Rev. 2.
- Richardson, I. G. *et al.*: 1987, *J. Geophys. Res.* **92**, 9997.
- Slavin, J. A., Lepping, R. P., and Baker, D. N.: 1990, *Geophys. Res. Letters* **17**, 913.
- Smith, E. J.: 1993, *EOS Transactions AGU* (Abstract SH 11 A-9) 234.
- Smith, E. J., Slavin, J. A., Zwickl, R. D., and Bame, S. J.: 1986, *Solar Wind-Magnetosphere Coupling*, Tokyo, p. 345.
- Sugiura, M.: 1965, *Radio Science* **69D**, 1133.
- Tsurutani, B. T., Gonzalez, W. D., Tang, F., Akasofu, S.-I., and Smith, E. J.: 1988, *J. Geophys. Res.* **93**, 8519.
- Tsurutani, B. T., Gonzalez, W. D., Tang, F., and Lee, Y. T.: 1992, *Geophys. Res. Letters* **19**, 73.
- Vinas, A. F. and Scudder, J. D.: 1986, *J. Geophys. Res.* **91**, 39.
- Whang, Y. C.: 1991, *Astrophys. J.* **377**, 255.
- Wilken, B., Goertz, C. K., Baker, D. N., Higbie, P. R., and Fritz, T. A.: 1982, *J. Geophys. Res.* **87**, 5901.
- Wilson, C. R. and Sugiura, M.: 1961, *J. Geophys. Res.* **66**, 4097.